J Mater Sci (2011) 46:6087–6095
DOI 10.1007/s10853-011-5571-z

Ion beam etching titanium for enhanced osteoblast response

Nicholas A. Riedel · John D. Williams · Ketul C. Popat

Received: 25 February 2011 / Accepted: 16 April 2011 / Published online: 7 May 2011

Abstract As the demand for hip and knee replacements continues to grow, researchers look to increase the operational lifetimes of these implants. Many implant failures are attributed to aseptic loosening caused from the repeated loading of these joints. It is believed that by improving the interface between the implant and natural tissue, implant life could be extended. This study evaluates the effects of argon ion etching on Ti6Al4V titanium alloy and the resulting implications this etching has on living cells. Three ion energies (300, 700, and 1100 eV) were used to etch the as-received titanium substrates. Topographical changes were examined by scanning electron microscopy. Etching at 700 and 1100 eV resulted in the formation of a hierarchical structure of micro/nano-texturization of micron-sized depressions with nano-structured ripples. A rat mesenchymal stem cell population was differentiated to an osteoblastic phenotype to test the biocompatibility of the surfaces. It was found that ion etching the titanium results in an improvement of early cellular activity and may enhance osteoblast performance.

Introduction

Over the past few decades, orthopedic procedures such as hip and knee replacements have become commonplace in most developed nations. It is estimated that by the year 2015, nearly 600,000 hip replacements and 1.4 million knee replacements will be performed in the United States alone [1]. Since these operations are both painful and costly, it would be ideal if the life of the implant exceeded the lifetime of the patient. Unfortunately, these replacement joints often become loose over time and require revision surgeries to re-secure or insert new hardware. The average expected in-service life of total knee replacements ranges from 10 to 15 years before a revision is required [2].

A number of factors influence the successes of these procedures including the competency of the surgeon and the risk of postoperative infections; however, the most critical issue is the interaction between the implant and the surrounding tissue. Direct bone–implant contact appears more advantageous than a fixation with the fibrous tissue that often forms after surgery [3, 4]. A weak or underdeveloped interface increases the chance the implant will loosen and a revision will be necessary [5]. In efforts to encourage healthy integration, researchers have focused on modifying the implant surfaces to enhance cellular responses in attempts to increase this osseointegration.

The most commonly proposed approaches to enhance implant integration are coating or texturizing the implant surface to trigger a directed cellular response. Bioactive implant coatings work on the premise of using chemical cues or protein bonding to promote cellular adhesion or activity. A few frequently used applications of this technique are surface functionalization with RGD peptides (to increase integrin binding and cellular adhesion) [6, 7] or coating the titanium with a calcium phosphate ceramic to mimic the environment of natural bone [8, 9]. Although these techniques have met some success, there are inherent problems to surface coatings as the issues of application, adhesion, durability, and lifetime often come into question.

N. A. Riedel · J. D. Williams
Department of Mechanical Engineering, Colorado State University, Fort Collins, CO 80523, USA

K. C. Popat (✉)
Department of Mechanical Engineering and School of Biomedical Engineering, Colorado State University, Fort Collins, CO 80523, USA
e-mail: Ketul.Popat@Colostate.edu

In efforts to avoid these problems, it would be beneficial to control cell response through the introduction of engineered surfaces. The hope is that a custom engineered surface could speed the rate of natural tissue regeneration and increase the bonded surface area between the implant and the living bone. It has been demonstrated on a number of different materials that the surface topography at the micro- and nano-scale has a direct effect on the behavior of cellular function [10–14]. A few methods of producing these topographies are photo lithography, colloidal lithography [15], electron beam lithography [16], ion beam lithography [17], extreme ultraviolet lithography [18], X-ray lithography [19], dip pen lithography [20], electrospinning [21, 22], and anodic oxidation [23]. Although these techniques are effective and produce a variety of surfaces, most are expensive, time consuming, and difficult to translate to a complex three-dimensional structure such as an implant.

A less recognized method for producing an ordered nano-structured surface topography is ion etching. Broad beam ion sources are already commonplace in the field of material processing; most often they are used to sputter targets in the creation of high quality thin films. They have also been used to intentionally modify the surface of material (i.e., exposing grain size in metals that are difficult to polish and/or chemically etch to reveal grain structure [24]). More recently it has been theorized and demonstrated that ion bombardment can produce uniform, highly ordered nano-features on various materials [25–31]. Since the topographies produced by this method are in many ways similar to the topographies produced by other tested models, it is reasonable to assume that ion bombarded surfaces may also be conducive to increase cellular adhesion and activity. This study examines the possibility that a titanium surface bombarded at normal incidence with argon ions can produce a surface capable of increasing osteoblast activity. Although this study uses a directed ion source to texturize the substrates, the underlying theory could be easily translated to complex geometries through the use of plasma immersion techniques [32].

Materials and methods

Substrates were prepared from 0.063 × 12 × 20″ medical grade Ti6Al4V-ELI sheets (Online Metal Supply). The metal sheets were sheared with a hydraulic press into workable substrates, approximately 1 × 1 cm. The substrates were cleaned ultrasonically in baths of Simple Green® solution, water, and finally acetone.

To etch the substrates, an 8-cm ion source was used to create a beam of energetic argon ions. The etching rate was controlled by adjusting the quantity and energy of the bombarding ions. For consistent processing, the beam current was constantly monitored and kept at 100 ± 10 mA. Since the ion distribution across the beam is not uniform, the substrates were placed on a rotating platform to ensure a uniform etch rate and equal exposure for all samples (Fig. 1). Three sets of 56 substrates were etched for 5 h with ion energies of 300, 700, or 1100 eV. Three substrates of each preparation were used in every biological evaluation ($n = 3$).

Weight measurements from a group of substrates ($n = 10$) processed at each condition were taken before and after processing to calculate the etch depth. Specifically, the etch rate was found using the density of Ti6Al4V-ELI ($\rho = 4.42$ g/cm^3), an assumed area $A = 1$ cm^2, the change in mass (Δm in grams), and the change in time (Δt in hours) using Eq. 1:

$$\text{Etch rate}_{\text{Calc}}\ (\text{nm/h}) = \frac{\Delta m}{\rho * A * \Delta t} * 10^7 \quad (1)$$

Theoretical values were calculated using the assumptions that ion current was 100 mA and uniform over the entire beam, beam area at the target was 16 cm in diameter (as measured from etched silhouette of the rotating platform), the density of the titanium alloy was 4.42 g/cm^3, and the substrates were only etched by the beam for one-fifth of the total time (due to the size of the rotating plate). These values were then converted to the appropriate units to provide ion current (j) in C/m^2 s and the density of titanium (ρ) in kg/m^3. Sputter yield data (Y in atoms/ion) was taken from Yamamura and Tawara [33]. The mass of a single titanium atom (m in kg/atom) and the charge of an electron (e in C) were also necessary.

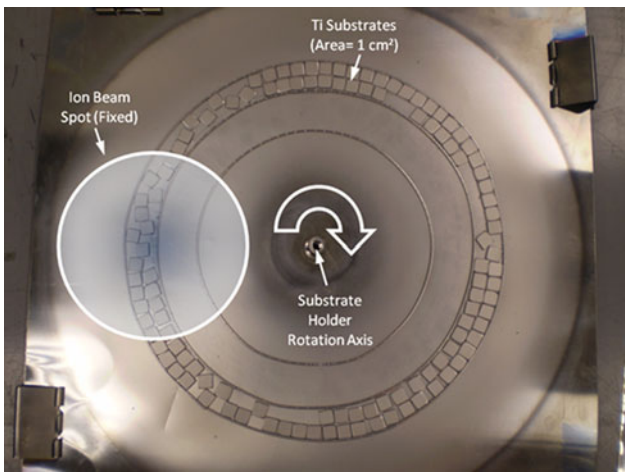

Fig. 1 Pictured is the substrate holder used during the etching of the samples. Since the ion beam is non-uniform, rotating the substrates through the beam in this manner ensures that a nearly identical path is followed by each substrate. This means the exposure time and dose of each sample is almost equal, providing a more uniform etch than setting the samples stationary under the beam

The equation used for the calculations of these theoretical values is shown in Eq. 2:

$$\text{Etch rate}_{\text{Theor}}\ (\text{nm/h}) = \frac{Y * j * m}{\rho * e} \quad (2)$$

Physical characterization

After etching, the surfaces of the substrates were examined with a JEOL JSM-6500F scanning electron microscopy (SEM) at a working distance of 10 cm and a voltage of 15 kV. The surfaces were plated with 5 nm of gold to ensure clear imaging.

Water contact angle measurements were also performed on the as-received and etched substrates. Using a FTA1000 B Class (First Ten Angstroms, Inc) contact angle machine, a droplet of distilled water, approximately 1.26 ± 0.05 μL was dropped onto each surface. Immediately after dropping, a camera level with the sample captured an image of the droplet. The image was then processed with the accompanying Fta32 software to give contact angle and droplet volume. Six samples from each preparation were tested ($n = 6$).

Cell culture

Cell isolation

In order to evaluate the mesenchymal stem cell (MSC) interaction with the substrates, the long bones (femur, humorous, and tibia) were aseptically harvested from two adult Wistar rats immediately after euthanasia. Using scissors and sterile technique, the ends of the bones were severed, and maintenance media [α-MEM with 10% fetal bovine serum (FBS, Sigma) and 1% penicillin/streptomycin (pen/strep, Sigma)] was flushed through the medullary cavity and collected. The media was then filtered through a 70 μm porous nylon filter into a clean centrifuge tube to remove any bone chips or other large unwanted debris. A hemocytometer was used to estimate the cell density of the filtered media. The celled media was then diluted to 1 million cells/mL through the addition of warmed fresh media. 1 mL of this concentration was seeded on each of the substrates. Before seeding, the substrates were cleaned with ethanol, sterilized under an ultraviolet lamp, and incubated in fresh media overnight.

Seeding and culture

The cultures were kept incubated in a sterile environment at simulated body conditions of 37 °C and 5% CO_2. On Day 4, 0.5 mL of the media was removed from the substrates and replaced with an equal amount of fresh media. A full media change was performed on Day 7 using a differentiation media [α-MEM supplemented with 10% FBS, 1% pen/strep, Dexamethasone (10^8 M), ascorbic acid (50 mg/mL), and β-glycerolphosphate (8 mmol)] to force the differentiation of the osteoprogenetor cells to an osteoblastic phenotype. This media was replaced every other day for the remainder of the study.

Short-term cell response

MTT assay

Early cellular activity was assessed on Day 1 and Day 4 through the use of a MTT (3-[4,5-dimethylthiazol-2-yl]-2,5-diphenyl tetrazolium bromide) assay (Sigma, CGD-1). The assay protocol provided by the company was followed. MTT solution was added to the maintenance media and allowed to incubate at 37 °C for 3 h. The mitochondrial dehydrogenases of productive cells cleaved the tetrazolium rings of the MTT solution and resulted in the formation of purple formazan crystals. These crystals were dissolved when the MTT solvent supplied in the kit was added to the solution in the wells. The substrate absorbance was measured spectrophotometrically at a wavelength of 570 nm through the use of a FLUOstar Omega (BMG Labtech). A background absorbance measured at 690 nm was subtracted from the original reading.

Calcein AM staining

Cell adhesion and spatial organization were assessed qualitatively through calcein AM (Invitrogen) fluorescence staining on Day 1, Day 4, and Day 7. Living cells use nonspecific cytosolic esterases to convert the non-fluorescent calcein AM to fluorescent calcein, which can then be examined. The maintenance media was aspirated, and the substrates were gently rinsed with phosphate buffer solution (PBS) to remove non-adherent cells. A 2 μM solution of calcein AM diluted in PBS was added to each well. To prevent photo-bleaching, the substrates were shielded from light until cells were imaged using appropriate filters on a Zeiss Axioplan 2 fluorescence microscope (Carl Zeiss).

SEM evaluation

Cell morphology was observed on Day 1, Day 4, and Day 7 by SEM. To prepare the substrates, the cells were placed in a solution of 3% glutaraldehyde (Sigma), 0.1 M sodium cacodylate (Polysciences, Warrington, PA), and 0.1 M sucrose (Sigma) for 45 min. Substrates were then soaked in buffer containing 0.1 M sodium cacodylate and 0.1 M sucrose. The cells were then dehydrated by soaking the substrates in increasing concentrations of ethanol (35, 50, 70, 95, and 100%) for 10 min each. Further dehydration

was achieved by soaking the substrates in hexamethyldisilazane (HMDS, Sigma) for 10 min. Before imaging, a 5 nm gold coating was deposited on the substrates to increase conductance of the surface to improve SEM resolution.

Long-term cell response

The osteoblast responses on the substrates were assessed once a week for 3 weeks after the forced differentiation. The time points used for evaluation were as follows: Week 1 (14 days into the study), Week 2 (21 days), and Week 3 (28 days). SEM evaluations of the surfaces were also performed at these time points using the same methodologies previously described.

ALP assay

Osteoblast activity was monitored through the use of an alkaline phosphatase (ALP) colorimetric assay (BioAssay Systems). The correlation between ALP and cellular activity could be made since ALP is a hydrolase enzyme produced as a byproduct of active osteoblasts. The titanium substrates were moved into fresh 24-well plates, and 1 mL of a cell lysis reagent (CelLytic M, Sigma) was added to each of the wells and gently shaken for 15 min at room temperature. This lysis reagent was then collected and added to a solution of *p*-nitrophenyl phosphate and magnesium acetate, prepared to kit specifications. The ALP present in the reagent causes a conversion of the *p*-nitrophenyl phosphate into yellow colored product (*p*-nitrophenol and phosphate). The reaction rate is directly proportional to the enzyme activity. Substrates were read twice ($t = 0$ min and $t = 4$ min) with a FLUOstar Omega (BMG Labtech) at a wavelength of 405 nm to determine this rate.

Results and discussion

Etched titanium substrate evaluation

Figure 2 shows the SEM images taken of the processed substrates. After etching the titanium substrates with various ion energies, it was obvious that the higher the energy of the ions, the more dramatically the surfaces were affected. Substrates etched at 300 eV showed little variation in surface topography from their pre-processed state. The low energy etching on these substrates only served to smooth the sharp imperfections created from the original manufacturing of the titanium sheets. However, the 700 and 1100 eV etched substrates yielded a unique topography that appeared to be highly dependent on the grain size and structure of the metal. These higher energies created hierarchical surfaces with uniform features at both the micro- and nano-scale. At the micro-scale, plateaus and valleys ranging in size from 5 to 15 μm were clearly distinguishable. Many edges of these features appeared to terminate at the grain boundaries of the alloy. This effect is clearly seen in Fig. 3. It has been observed previously that the orientation of the crystal structure affects how susceptible each grain is to etching [34]. Similarly, we believe that the micro-scale coarseness observed is a direct result of an uneven etching of individual grains.

At the nano-scale, the etching resulted in the formation of regularly spaced ripples, approximately 20 nm apart. The prominence of the nano-features was dependant on the ion energy; the higher the ion energy, the more pronounced the ripples. The 1100 eV etching consistently created well-defined ripple morphology, while the 700 eV etch resulted in definition ranging from barely visible to clearly apparent. The differences in ripple morphology from the two higher ion energies are illustrated in Fig. 4. The phenomenon of wave formation has also been reported when argon was used to sputter copper [35] and silver [36]. Ripple formation on the silver substrates was noted to occur at ion energies greater than 800 eV with substrate temperatures ranging from 270 to 320 K [36]. In this study, substrate temperature was not monitored, but the formation of ripples was only apparent on the 700 and 1100 eV substrates. The theory behind the evolution of these features has been described previously by Bradley and Harper [37].

Although these ripples were apparent over most of the etched surface, not all grains showed these formations. Figure 5 illustrates the differences observed between two bordering grains. Again, this disparity is likely due to variations in orientation of the crystal structure of the alloy and the resulting differences in susceptibility for atomic rearrangement of the surface.

The average change in mass measured for each ion energy was used to calculate the rate of etching. The results are shown in Table 1. Although there were discrepancies between the calculated and theoretical etch rates, this is not unexpected. The theoretical calculations were made based on the sputtering yields reported by previous researchers with varying methods of etching and measuring the sputter yields. These comparisons were made merely to ensure the results seen were reasonable. The total depth of etching during the 5 h long process ranged from 550 to 2,300 nm as the ion energy was varied from 300 to 1100 eV. Naturally, the most energetic ions resulted in the highest etch rate.

The water contact angle remained largely unaffected by the argon processing, and these results are given in Table 2. Since the contact angles are similar, this indicates that the substrates have comparable surface energies. There

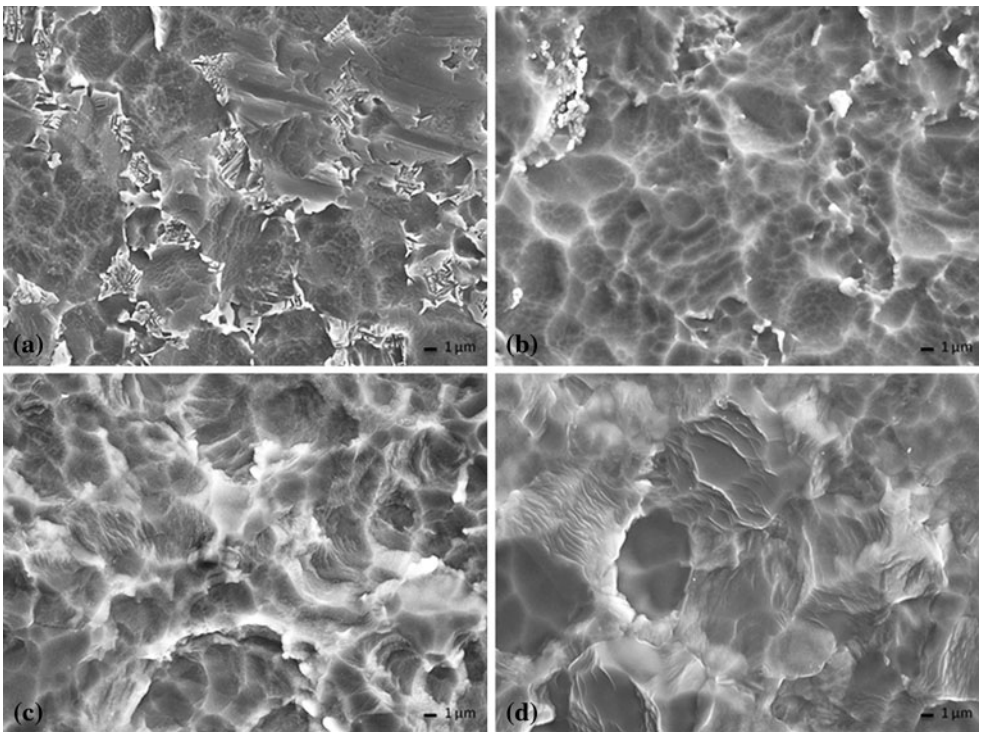

Fig. 2 These SEM images are representative of the surfaces produced by the argon etching (×4000). (**a**) The unmodified, as-received titanium used for processing and the study control. (**b**) Titanium substrate after 300 eV etch. (**c**) Titanium substrate after 700 eV etch. (**d**) Titanium substrate after 1100 eV etch

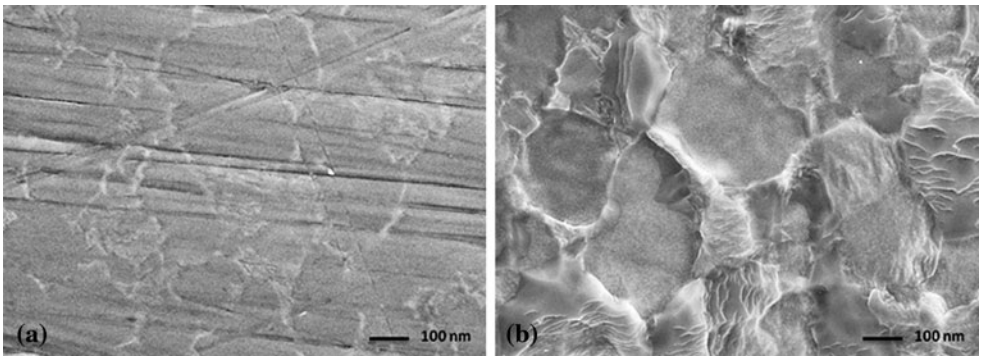

Fig. 3 SEM images comparing a polished Ti substrate (**a**) to a substrate etched at 1100 eV (**b**). The features apparent in the etched sample are of similar size and shape to the grain boundaries of the titanium observed on the polished substrate (exposed by minor chemical etch)

should be no loss of cellular adhesion on the etched substrates due to a drastic change in free energy.

Short-term cell response

The substrates were seeded with a rat MSC population to evaluate the effects of the hierarchical structure on cellular response. Short-term evaluation of the MSC reactions to the surfaces began 1 day after seeding. Calcein AM staining indicated that the cells were able to attach and remain viable across the surface of all the substrates. Figure 6 shows representative images of the substrates. On Day 1, the number of adherent cells was similar on all of the substrates, except the substrates etched at 1100 eV which displayed notably fewer cells. This trend continued over Day 4 and Day 7; the substrates etched at the highest energy consistently displayed fewer adhered cells. It is possible that the rougher nature of the 1100 eV surface was responsible. Cell densities appeared comparable on the 300 eV etched, 700 eV etched, and untreated titanium throughout the evaluation.

The cellular reactions on the 300 eV etched surfaces were similar to those of the 700 eV etched substrates. As early as Day 4, the cells on these substrates were grouping,

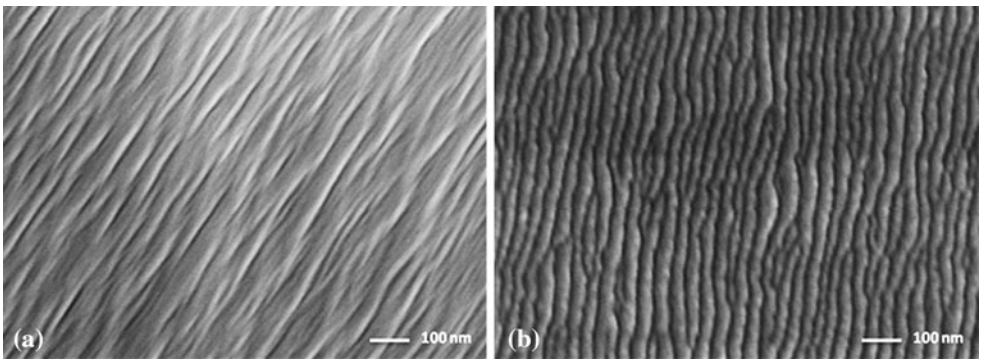

Fig. 4 SEM images of the surfaces taken at ×100,000 resolution. (**a**) Weak ripple formation apparent on the surface of a titanium substrate etched at 700 eV. (**b**) Fully developed ripples formed on the substrate etched at 1100 eV

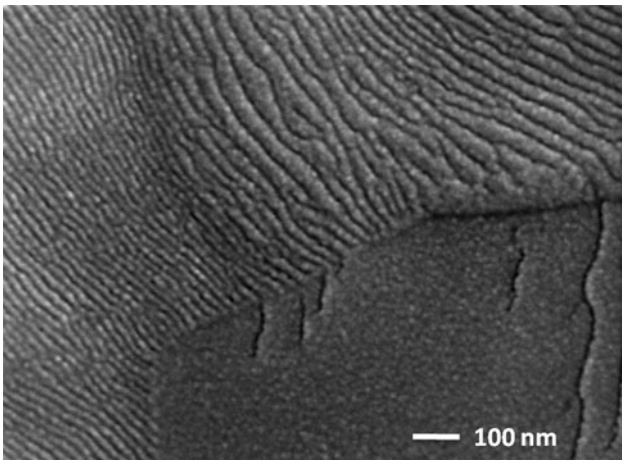

Fig. 5 This image displays the grain dependent contrast of the ripple formation produced by a 700 eV ion etch. Although the rippled nanotopography was produced across most the surface, some grains displayed a resistance. It is probable that some crystallographic orientations inhibit the bombarding ions from causing the atomic rearrangement necessary for these formations to occur

Table 1 Calculated etch rates for the varying ion energies

	300 eV	700 eV	1100 eV
Calculated etch rate (depth of etch) (nm/h)	108.6	162.9	447.9
Theoretical etch rate (depth of etch) (nm/h)	124	238	310

and advanced spreading was evident. By Day 7, the cells on the 300 and 700 eV substrates were highly spread, while most cells on the untreated titanium remained in a rounded morphology. This indicates that the topography created by argon ion bombardment at 300 and 700 eV had a high cellular affinity and allowed cellular migration.

The results from the MTT colorimetric assay are displayed in Fig. 7. At Day 1, there appeared similar mitochondrial activity on all substrates. The substrates etched at 1100 eV showed slightly more activity than those etched at the lower energies. This result is surprising for the given the calcein AM staining showed that the higher energy substrates appeared to maintain fewer living cells. The trend observed on Day 1 continued into Day 4. The 300 and 700 eV substrates had absorbance values slightly lower than those of the control, while the 1100 eV substrates performed at levels comparable to the unprocessed titanium.

Initial cellular adhesion appeared consistent for all the substrates with the cells maintaining a rounded morphology. By Day 4, the adhered cells were beginning to exhibit a spread morphology on the surface and network with adjacent cells. Behavior was similar for all substrates except those etched at 1100 eV, which seemed to maintain rounded cell morphologies. In 7 days, cell densities had increased, and the morphology was increasingly spread. Figure 8 displays the representative images taken at Day 7. These images confirm the results seen with the Calcein staining, where the cells on the etched substrates demonstrated a higher degree of spreading and appeared to be better adhered to the surface.

Long-term cell response

Alkaline phosphatase, an enzyme present in the matrix vesicles deposited by osteoblasts, is thought to play a direct role in the induction of hydroxyapatite deposition [38]. In the early stages of biomineralization, ALP is upregulated to supply inorganic phosphates for the mineralization process. However, once mineralization begins, the ALP levels drop before a mature mineralized matrix is formed [39]. These fluctuations in ALP levels have been observed in similar studies [40, 41]. The ALP results from this study are given in Fig. 9. Although these readings are not normalized, the values can still be considered representative of osteoblast performance since SEM evaluations of the surfaces suggest similar cell quantities on almost all substrates after the first week. At all time points, the as-received substrates were

Table 2 Results from the water contact angle testing

	Control Ti	300 eV	700 eV	1100 eV
Contact angle (°)	54.55 ± 6.54	56.72 ± 4.06	62.85 ± 0.98	58.52 ± 2.02

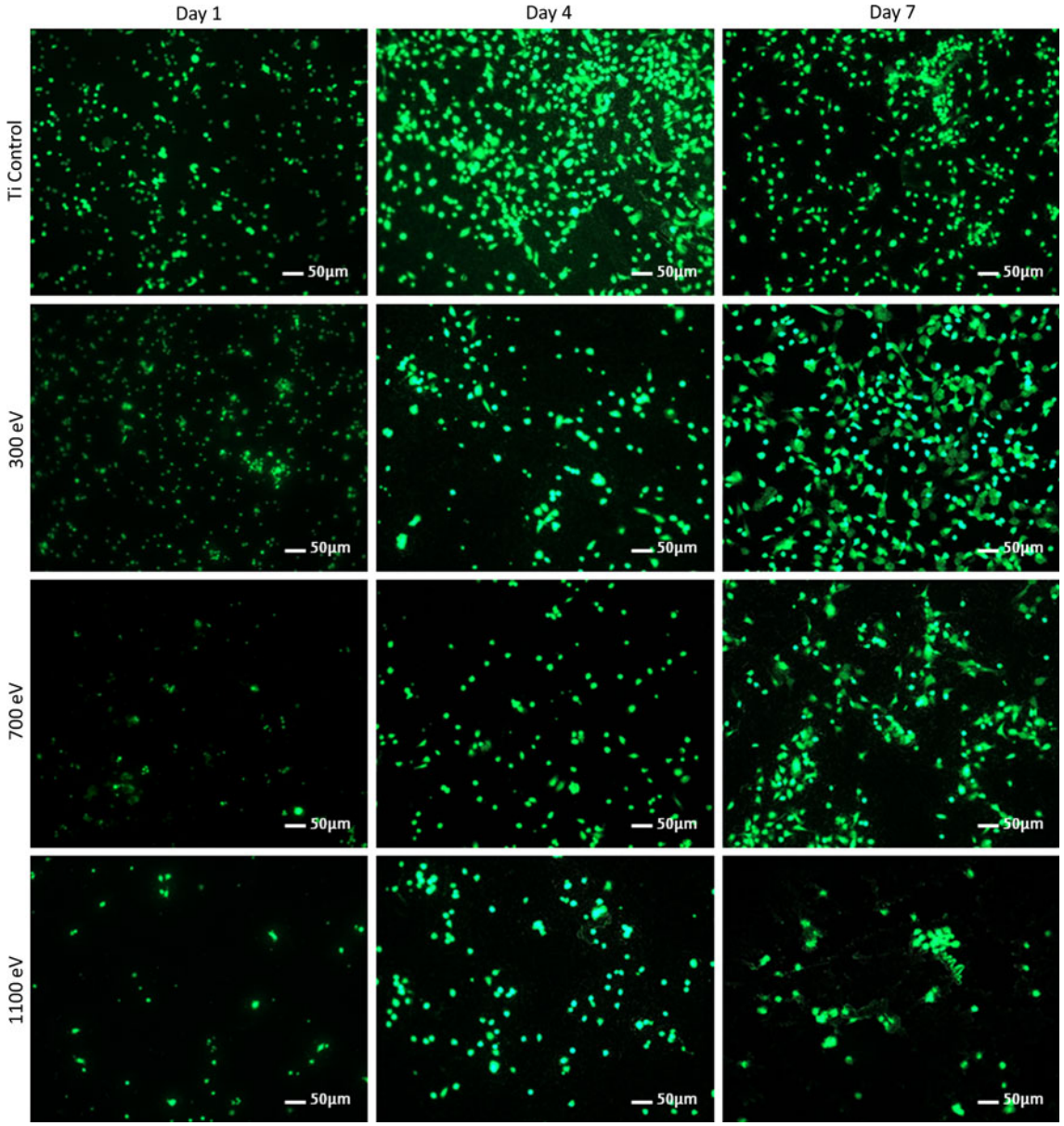

Fig. 6 These are representative images from the calcein AM cell staining. The control group and 300 eV etched substrates maintained a fairly dense cell population through the course of the first week. Initial attachment on the 700 and 1100 eV substrates was not as good. By Day 7, only the 1100 eV substrate still had fewer cells than the other samples. Also by Day 7, the 300 and 700 eV preparations were displaying advanced spreading, while the cells on the control and 1100 eV substrates maintained a mostly rounded morphology

consistently poor performers compared to the etched substrates. Unfortunately, the errors associated with these measurements were too large to draw any definitive conclusions, though there was a perceived increase in ALP activity on all the etched samples. The as-received substrates all performed similarly while there were large variations in the etched samples. The lower values in the etched samples were similar to those seen in the untreated titanium, while the higher values were up to five times higher. Large standard deviations resulted from wide fluctuations in measured ALP values and low sample numbers. It is probable that the etching increases

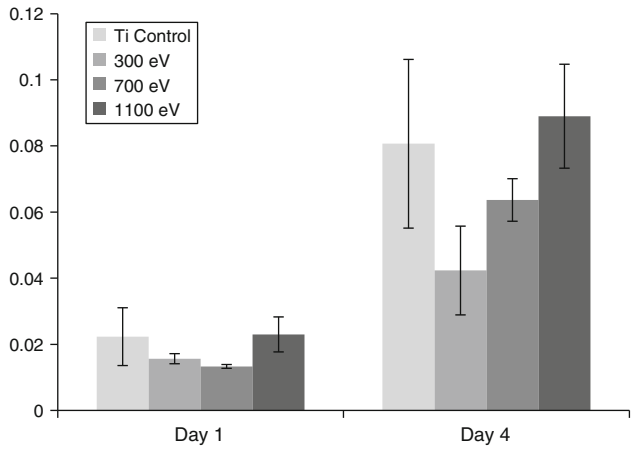

Fig. 7 MTT results for the Day 1 evaluation indicate similar cellular activity levels on all the preparations. Day 4 results display variation in the etched samples, but all levels are still comparable to the activity on the control

osteoblast activity, though suggestive, these results are not conclusive.

The SEM images taken over the long-term evaluation showed that cellular reactions on these surfaces were similar across the duration of the study. The substrates had cell densities that were approximately equal in number with cells exhibiting similar conformation and spreading.

Conclusions

Normal incidence argon ion etching was able to produce a hierarchical topography on a titanium surface. At energies of 700 and 1100 eV, the surfaces had plateaus and valleys ranging from 5 to 15 μm, while at the nano-scale regularly spaced ripples ($\sim$20 nm apart) were observed. The etching had a largely positive impact on the cellular interaction over the as-received substrates. Calcein AM staining and SEM imaging confirmed that there was an increase in early cell spreading and mobility. This is likely due to a combination of the imparted nano-texturization and the erosion of large physical obstacles by ion bombardment. The etched substrates had slightly lower but comparable MTT absorbances to the untreated as-received substrates, but the ALP values of the etched were higher. It can be concluded that the argon beam etching provided some improvement, though not dramatic, in the performance over the as-received substrates.

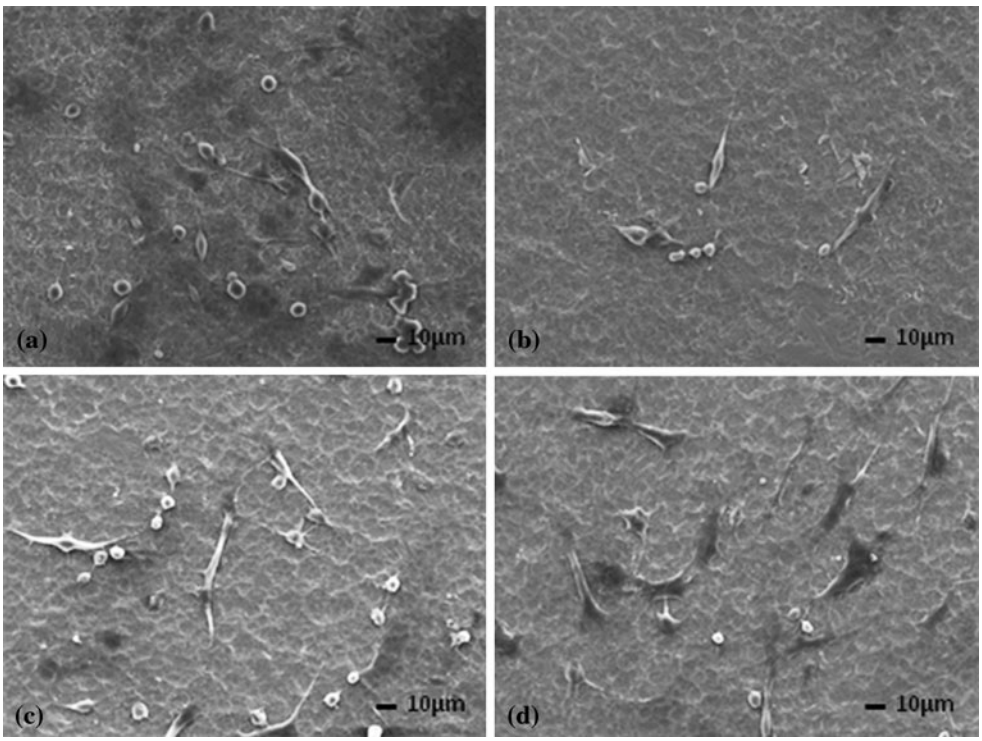

Fig. 8 Representative SEM images taken from the Week 3 evaluation of the substrates (×500). (**a**) Many cells on the control surface have maintained a rounded morphology. (**b**) The 300 eV etched substrate displayed fewer cells than the control surface, but most cells were well spread on the surface. (**c**) The 700 eV substrate displayed similar cell quantities to the control surface, but more cells were in a highly spread morphology typical of osteoblasts. (**d**) The reaction on the 1100 eV substrate was nearly identical to the reaction on the 700 eV surface

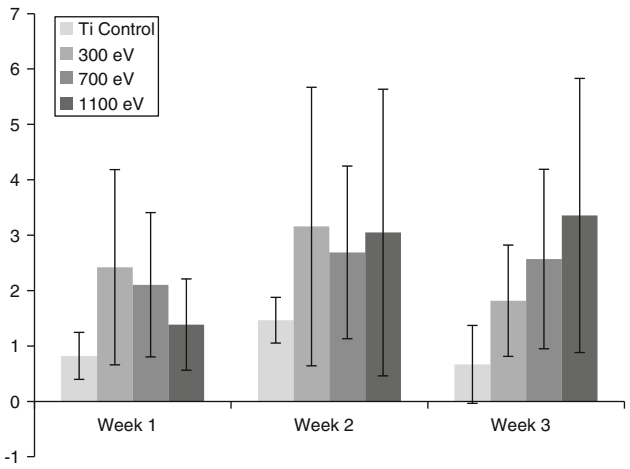

Fig. 9 ALP responses indicated higher average values on the etched substrates in all cases; however, the standard deviations of the measurements were too large on the sample size of three to draw any statistically significant conclusions on whether activity was really increased

Acknowledgements The authors wish to thank Dr. Timothy Ruckh for his assistance with harvesting the mesenchymal stem cells, as well as Dr. Cody Farnell and Dr. Casey Farnell for their consultation and support of the ion sputtering process. We would also like to thank Abound Solar for the use of their contact angle testing equipment.

References

1. Kim S (2008) Arthritis Rheum 59:481
2. Fehring TK, Odum S, Griffin WL, Mason JB, Nadaud M (2001) Clin Orthop Relat Res 392:315
3. Linder L, Carlsson A, Marsal L, Bjursten LM, Branemark PI (1988) J Bone Joint Surg Br 70:550
4. Branemark PI, Hansson BO, Adell R et al (1977) Scand J Plast Reconstr Surg 16:1
5. Sharkey PF, Hozack WJ, Rothman RH, Shastri S, Jacoby SM (2002) Clin Orthop Relat Res 404:7
6. Schliephake H, Scharnweber D, Dard M, Sewing A, Aref A, Roessler S (2005) J Biomed Mater Res B 73B:88
7. Ferris DM, Moodie GD, Dimond PM, Gioranni CW, Ehrlich MG, Valentini RF (1999) Biomaterials 20:2323
8. Dumbleton J, Manley MT (2004) J Bone Joint Surg Am 86-A:2526
9. Barrere F, van Blitterswijk CA, de Groot K (2006) Int J Nanomed 1:317
10. Mendonca G, Mendonca DB, Aragao FJ, Cooper LF (2008) Biomaterials 29:3822
11. Dalby MJ, McCloy D, Robertson M et al (2006) Biomaterials 27:2980
12. Price RL, Haberstroh KM, Webster TJ (2003) Med Biol Eng Comput 41:372
13. Rekow D, Van Thompson P, Ricci JL (2006) J Mater Sci 41:5113. doi:10.1007/s10853-006-0071-2
14. Colombo P, Vakifahmetoglu C, Costacurta S (2010) J Mater Sci 45:5425. doi:10.1007/s10853-010-4708-9
15. Hanarp P, Sutherland DS, Gold J, Kasemo B (2003) Colloid Surf A 214:23
16. Vieu C, Carcenac F, Pepin A et al (2000) Appl Surf Sci 164:111
17. Morimoto H, Sasaki Y, Saitoh K, Watakabe Y, Kato T (1986) Microelectron Eng 4:163
18. Gan J, Chen H, Zhou F et al (2010) Colloids Surf B Biointerfaces 76:381
19. Romanato F, Tormen M, Businaro L et al (2004) Microelectron Eng 73–74:870
20. Piner RD, Zhu J, Xu F, Hong S, Mirkin CA (1999) Science 283:661
21. WJ Li, Laurencin CT, Caterson EJ, Tuan RS, Ko FK (2002) J Biomed Mater Res 60:613
22. Zhou FL, Gong RH, Porat I (2009) J Mater Sci 44:5501. doi:10.1007/s10853-009-3768-1
23. Popat KC, Leoni L, Grimes CA, Desai TA (2007) Biomaterials 28:3188
24. Malhotra ML (1977) Metallography 10:337
25. Facsko S, Dekorsy T, Koerdt C et al (1999) Science 285:1551
26. Ziberi B, Cornejo M, Frost F, Rauschenbach B (2009) J Phys Condens Matter 21:224002
27. Reiche R, Hauffe W (2000) Appl Surf Sci 165:279
28. Wei QM, Zhou XL, Joshi B et al (2009) Adv Mater 21:2865
29. Frost F, Schindler A, Bigl F (2000) Phys Rev Lett 85:4116
30. Toma A, de Mongeot FB, Buzio R et al (2005) Nucl Instrum Methods B 230:551
31. Makh SS, Smith R, Walls JM (1982) J Mater Sci 17:1689. doi:10.1007/BF00540797
32. Pelletier J, Anders A (2005) IEEE Trans Plasma Sci 33:1944
33. Yamamura Y, Tawara H (1996) Atom Data Nucl Data 62:149
34. Batic BS, Jenko M (2010) J Vac Sci Technol A 28:741
35. Rusponi S, Costantini G, Boragno C, Valbusa U (1998) Phys Rev Lett 81:4184
36. Rusponi S, Boragno C, Valbusa U (1997) Phys Rev Lett 78:2795
37. Bradley RM, Harper JME (1988) J Vac Sci Technol A 6:2390
38. Anderson HC (2003) Curr Rheumatol Rep 5:222
39. Boyan BD, Schwartz Z, Swain LD (1992) Bone Miner 17:263
40. Shin H, Zygourakis K, Farach-Carson MC, Yaszemski MJ, Mikos AG (2004) J Biomed Mater Res A 69:535
41. Bancroft GN, Sikavitsas VI, van den Dolder J et al (2002) Proc Natl Acad Sci USA 99:12600